ARMY RESEARCH LABORATORY

Development of Nanoenergetic Micro-fluidic Jet Injectors

by Clay S. Staley, Christopher J. Morris, and Luke J. Currano

ARL-TR-5872 **January 2012**

NOTICES

Disclaimers

The findings in this report are not to be construed as an official Department of the Army position unless so designated by other authorized documents.

Citation of manufacturer's or trade names does not constitute an official endorsement or approval of the use thereof.

Destroy this report when it is no longer needed. Do not return it to the originator.

Army Research Laboratory
Adelphi, MD 20783-1197

ARL-TR-5872 **January 2012**

Development of Nanoenergetic Micro-fluidic Jet Injectors

Clay S. Staley, Christopher J. Morris, and Luke J. Currano
Sensors and Electron Devices Directorate, ARL

REPORT DOCUMENTATION PAGE

Form Approved
OMB No. 0704-0188

1. REPORT DATE *(DD-MM-YYYY)*	2. REPORT TYPE	3. DATES COVERED (From - To)
January 2012	Final	June 2011 to August 2011

4. TITLE AND SUBTITLE
Development of Nanoenergetic Micro-fluidic Jet Injectors

5a. CONTRACT NUMBER
W911NF-07-2-0027

5b. GRANT NUMBER

5c. PROGRAM ELEMENT NUMBER

6. AUTHOR(S)
Clay S. Staley, Christopher J. Morris, and Luke J. Currano

5d. PROJECT NUMBER

5e. TASK NUMBER

5f. WORK UNIT NUMBER

7. PERFORMING ORGANIZATION NAME(S) AND ADDRESS(ES)
U.S. Army Research Laboratory
ATTN: RDRL-SER-L
2800 Powder Mill Road
Adelphi, MD 20783-1197

8. PERFORMING ORGANIZATION REPORT NUMBER
ARL-TR-5872

9. SPONSORING/MONITORING AGENCY NAME(S) AND ADDRESS(ES)

10. SPONSOR/MONITOR'S ACRONYM(S)

11. SPONSOR/MONITOR'S REPORT NUMBER(S)

12. DISTRIBUTION/AVAILABILITY STATEMENT
Approved for public release; distribution unlimited.

13. SUPPLEMENTARY NOTES

14. ABSTRACT
We present the fabrication, assembly, and packaging of first generation nanoenergetic fluidic jet generators. The generators consist of an energetic material chamber, elastic piston, vaccine reservoir, and convergent nozzle cap all tightly bonded in a self-contained device using micro-electromechanical system (MEMS) processing techniques. Maximum deformation lengths of the polydimethylsiloxane (PDMS) membranes are characterized as a function of PDMS diameter, PDMS thickness, energetic material composition, and energetic material mass using high-speed photography and compared with theoretical calculations. Assembled nanoenergetic fluidic jet generators are analyzed to extract critical operation parameters such as fluidic jet velocity, ejected jet diameter, penetration depth, and fluidic dispersion using in air jet velocity measurements and ballistic gel penetration characterization. Performance scaling laws have been established to determine design parameters for smaller future generation devices.

15. SUBJECT TERMS
Nanoporous silicon, nanothermites, needle-free drug deliver

16. SECURITY CLASSIFICATION OF:			17. LIMITATION OF ABSTRACT	18. NUMBER OF PAGES	19a. NAME OF RESPONSIBLE PERSON
a. REPORT	b. ABSTRACT	c. THIS PAGE			Christopher J. Morris
Unclassified	Unclassified	Unclassified	UU	20	19b. TELEPHONE NUMBER (*Include area code*) (301) 394-0950

Standard Form 298 (Rev. 8/98)
Prescribed by ANSI Std. Z39.18

Contents

List of Figures

Acknowledgments

We wish to acknowledge technical guidance from Dr. Luke Currano and Dr. Shubhra Gangopadhyay. We would also like to acknowledge Mr. Brian Isaacson for technical assistance during wafer processing and the U.S. Army Research Laboratory cleanroom staff for providing the resources necessary to accomplish this research.

Student Bio

Mr. Clay Stephen Staley is currently pursuing a doctoral degree in electrical engineering at the University of Missouri-Columbia under the advisory of Dr. Shubhra Gangopadhyay. He acquired a bachelor of science in electrical engineering from the University of Missouri on December 2009. The crux of his research is the integration of nanoenergetic materials with micro-device fabrication and applied technologies. Mr. Staley has worked on nanoenergetic materials synthesis and characterization, micro-thruster propulsion systems, shockwave-induced drug transfection, chip disruption information security systems, micro-initiator platforms, environmentally friendly secondary propellant initiators, and nanoenergetic needle-free vaccine injection. In the future, Mr. Staley will continue basic scientific research using nanoenergetic materials packaged in micro-devices to develop innovative approaches towards solving fundamental challenges present in the scientific community. He hopes to facilitate the transition of his research to field readiness levels in an effort to satisfy real-world commercial and military application demands.

1. Introduction and Background

Needle-free liquid jet injectors were invented more than 60 years ago for the delivery of proteins and vaccines (*1, 2*). The concept of operation behind needle-free injectors is to provide transdermal injection by forcing liquid through a tiny orifice that is held against the skin. This creates a very fine, high-velocity stream of medication that penetrates the skin. The process of needle-free injection in illustrated in figure 1.

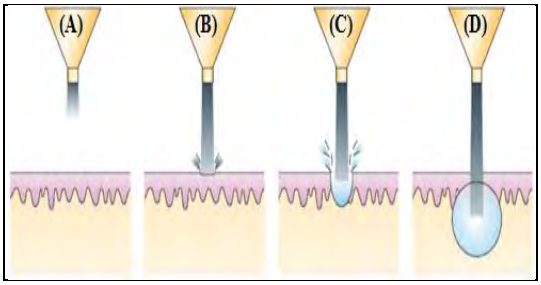

Figure 1. Illustration of needle-free transdermal injection process (*3*).

Typically, needle-free injection systems are driven by compressed gas or a spring-loaded piston. An alternative to traditional liquid jet generators is a device driven by the rapid combustion of nanoenergetic material, defined as an exothermic reaction between particles having characteristic dimensions of 1–100 nm. Such a device is similar to one driven by compressed gas in that the impulse arises from the rapid release and expansion of gases. However, a pellet of solid nanoenergetic material harbors greater energy and power density than an equally sized compressed gas cylinder, and greater than many other energy storage technologies, as shown in figure 2.

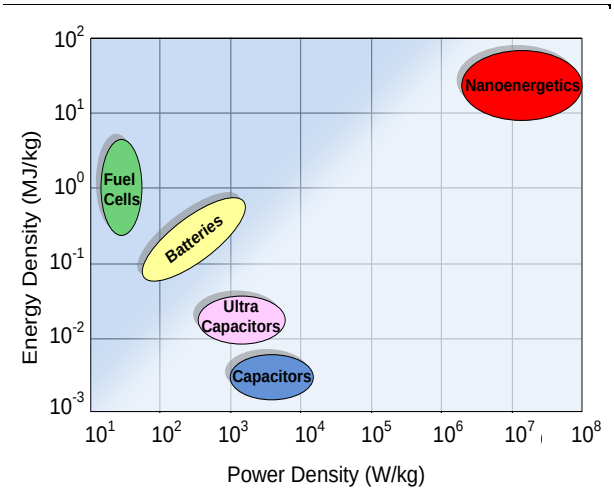

Figure 2. Energy density vs. power density of various energy sources compared to nanoenergetic materials (*4–6*).

Nanoenergetic materials can be integrated with micro-electromechanical system (MEMS) and solid-state electronics to fabricate millimeter- or micrometer-scale liquid jet generators. Ideally, by fabricating micro-injection devices, traditional pitfalls associated with commercially available needle-free jet injectors, such as the causation of bruising and abrasions, inconsistent vaccine dose delivery, and the requirement of a trained administrator, may all be addressed. The fundamental device design to accommodate nanoenergetic actuation incorporates an energetic material chamber and fluid reservoir separated by an elastic piston membrane. The reaction and expansion of the energetic material pushes the membrane and applies pressure to the fluid chamber ejecting fluid from the reservoir. The elastic membrane prevents reactants from interfering with the fluid or the injection recipient, and also provides a thermal barrier preventing the transfer of heat and, if necessary, light to the fluid. Output fluidic jet power can be modulated by adjusting the energetic material formulations and quantities, and reaction rates can be modulated to minimize any heat transfer to the surrounding system.

2. Experiment and Calculations

Prior to designing and fabricating nanoenergetic micro-fluidic jet injectors, device volumes, nanoenergetic mass loaded, and elastic membrane thickness need to be considered. To establish design parameters for device fabrication, first-order approximations were conducted to determine maximum elastic diaphragm deflection and mechanical stresses incurred in response to applied transient pressures. Polydimethylsiloxane (PDMS) was chosen as the elastic membrane material owing to a high elasticity and maturity of use in MEMS processing. Copper oxide-aluminum (CuO/Al) nanothermite was selected as the nanoenergetic material for this study. First, the volume of gas liberated from the combustion of a CuO/Al mass at standard temperature and pressure (273.15 K and 101.325 kPA) is extracted through the ideal gas law expressed as

$$V_1 = \frac{n_1 R T_1}{P_1}, \tag{1}$$

where V_1 is the volume of gas generated in an unconfined environment, n_1 is the amount of gas in moles calculated from the theoretical gas evolved during CuO/Al decomposition equal to 0.0054 mol/g, R is the universal gas constant, T_1 is standard temperature, and P_1 is standard pressure (*7, 8*). Assuming an isochoric combustion process, the uniform pressure exerted on an energetic material reservoir of volume V_2 is given as

$$P_2 = \frac{P_1 V_1 T_2}{V_2 T_1}, \tag{2}$$

where P_2 is the material reservoir pressure and T_2 is the adiabatic flame temperature of the CuO/Al nanothermite given as 2570 °C (*7, 8*). By evaluating equations 1 and 2 for a range of

CuO/Al mass contained in a chamber volume of 1.57 mm^3 at 20% Theoretical Maximum Density (TMD), a linear relationship is extracted to determine pressure generated versus material mass expressed as

$$P = (81.26\ \text{MPa/mg})\,m - 7.105\ \text{MPa}\,, \tag{3}$$

where P is reaction pressure and m is mass of CuO/Al (in mg) loaded into the containment volume. The density for slurry deposited nanothermite materials as prepared in this work is approximately 20% TMD and is accounted for here to ensure an experimentally practical range of CuO/Al mass is used in the calculation.

To approximate maximum PDMS diaphragm deflection as a function of applied pressure, the mechanical behaviors of the diaphragm are modeled as a disc with clamped edges as shown in figure 3.

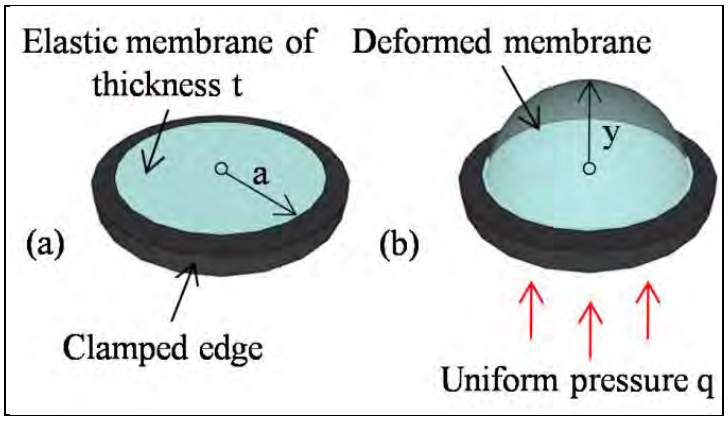

Figure 3. Illustration of elastic membrane modeling: (a) unstressed elastic membrane previous to pressure input and (b) elastic membrane deformation in response to uniform pressure q.

The maximum deflection of the membrane resulting from the application of a uniform pressure is calculated using the expression

$$\frac{qa^4}{Et^4} = K_1\frac{y}{t} + K_2\left(\frac{y}{t}\right)^3, \tag{4}$$

where q is the pressure applied, a is disc radius, E is Young's modulus, t is disc thickness, and y is the maximum deflection distance at the center of the disc. K_1 and K_2 are parameters calculated from the following equations (*9*):

$$K_1 = \frac{5.33}{1-\nu^2}, \tag{5}$$

$$K_2 = \frac{2.6}{1-\nu^2}, \tag{6}$$

where ν is Poisson's ratio of the disc material. To evaluate equations 4, 5, and 6 a Young's modulus and Poisson's ratio for Sylgard 184 PDMS (prepared using 10 parts silicone base to 1 part curing agent) of 1.8 MPa and 0.45, respectively, were used (*10*). With a known maximum deflection distance, the mechanical flexure and tension stresses combined are evaluated against the ultimate yield strength for PDMS equal to 8 MPa (*11*) to determine if the diaphragm will rupture during actuation. The combined diaphragm stresses are calculated from the equation

$$\frac{\sigma a^2}{Et^2} = K_3 \frac{y}{t} + K_4 \left(\frac{y}{t}\right)^2, \tag{7}$$

where σ is the combination of tension and flexure stresses (*9*). K_3 and K_4 are constants for a Poisson's ratio of 0.45, given as 3.64 and 0.98, respectively, for stress calculation at the center of the disc or as 7.27 and 1.73, respectively, for calculating stress at the edges of the disc. Equation 7 was evaluated for 1.57 mm^3 devices under the conditions of edge stresses as the edge stress magnitude will always be higher than the stresses at the center of the disc in this particular physical configuration. PDMS deflection and tension/flexure edge stress versus CuO/Al nanothermite mass for varied thickness PDMS membranes with a 1-mm radius are plotted in figure 4.

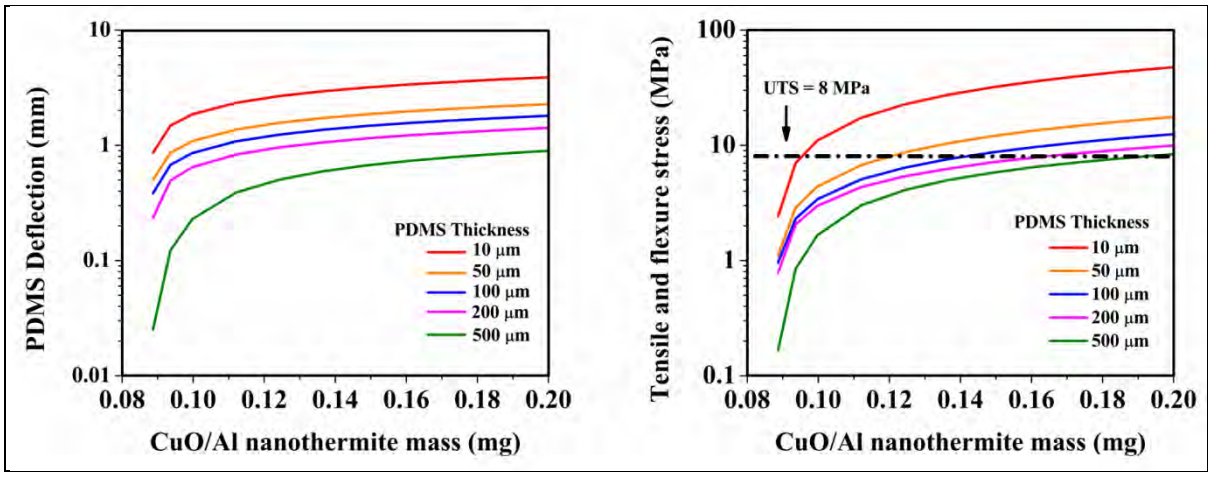

Figure 4. PDMS mechanical modeling: PDMS membrane deflection (left) and tension/flexture edge stress (right) as a function of CuO/Al mass and PDMS diaphragm thickness.

From this analysis, devices were designed to operate at maximum tensile and flexure stresses of approximately 4 MPa, which is half the value of the ultimate tensile strength for PDMS. The maximum deflection of the PDMS membrane will be engineered to be as large as possible without breaching membrane stresses of greater than 4 MPa. Material chamber and fluid reservoir diameters of 2 mm, 2.5 mm, and 3 mm were subsequently used for this study.

To prepare CuO/Al nanothermite, copper chloride $(CuCl_2)\cdot 2H_20$ powder, polyethylene glycol (PEG)-400, and sodium hydroxide (NaOH) flakes were purchased from Sigma Aldrich and used as received for CuO nanorod synthesis. The three chemicals were mixed and ground together

following a weight ratio of 1.7 $CuCl_2 \cdot 2H_20$: 1 NaOH: 2.3 PEG-400 via mortar and pestle, initiating the following reactions:

$$CuCl_2 + 2NaOH \rightarrow Cu(OH)_2 + 2NaCl \quad (8)$$

$$Cu(OH)_2 \rightarrow CuO + H_2O + \Delta H. \quad (9)$$

The reaction of $CuCl_2$ with NaOH yields copper hydroxide (CuOH) and sodium chloride (NaCl). Unstable CuOH then hydrolyzes in an exothermic process to yield CuO as a viscous, black paste. PEG-400 serves as a polymer surfactant in the process by coating the CuO nanorods to influence their growth geometry and prevent undesirable macro-structure formulations by occupying potential binding sites. A PEG-coated CuO slurry was then washed multiple times in 800 mL of deionized (DI) water through ultrasonic agitation for 1 h, left to settle, and drained until all PEG-400 surfactant was removed from the mixture. Wet CuO nanorods were then extracted from the solution onto fine porosity filtration paper using a suction filtration assembly and left to dry under vacuum, yielding primed CuO nanorods. A flow sheet for CuO nanorod synthesis is shown in figure 5.

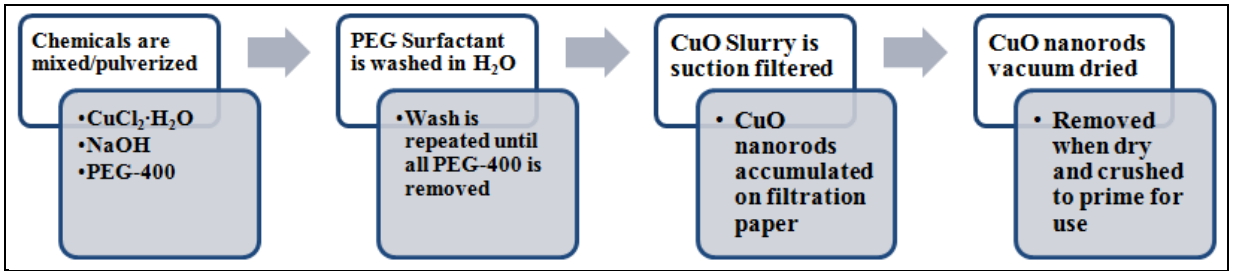

Figure 5. CuO nanorod synthesis flow sheet.

As prepared CuO was then placed in a scintillation vial and dispersed uniformly in 1.2 mL of isopropyl alcohol. Al nanoparticles purchased and used as received from Novacentrix (80 nm diameter, 80% active Al content, and a 2–3 nm aluminum oxide [Al_2O_3] passivation coating) were added to the solution in a weight ratio of 1 Al: 1.22 CuO. The slurry was then agitated in an ultrasonic bath for 4 h to allow for the self assembly of the Al nanoparticles onto the exposed CuO nanorod surface areas, producing an intimately and homogenously mixed CuO/Al nanothermite slurry suspended in isopropyl alcohol.

3. Results and Discussion

Nanothermite actuated micro-fluidic injectors were assembled from four separately processed silicon (Si) wafers consisting of an ignition substrate (with an integrated electro-thermal heating unit), an energetic material chamber, fluid reservoir, and convergent nozzle cap with a 150-μm-diameter orifice, as illustrated in figure 6.

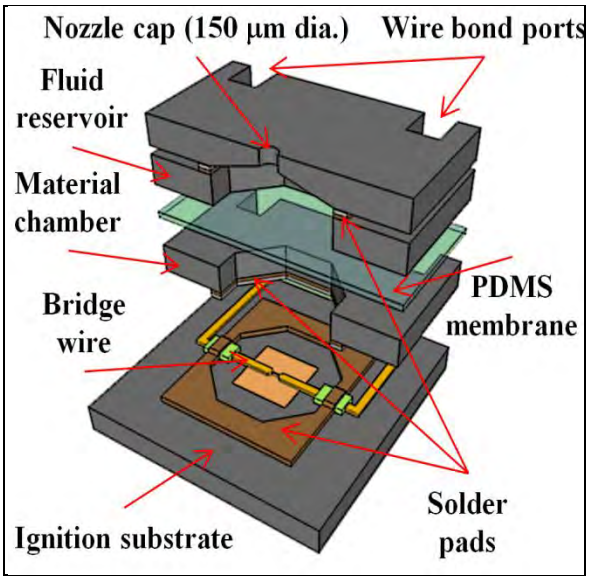

Figure 6. Cross-sectional illustration of micro-fluidic injector assembly.

To begin device fabrication, a p-type [100] orientation Si wafer double side coated with 600-nm-thick films of silicon nitride (Si_3N_4) was used for ignition substrate fabrication. Si_3N_4 from the backside of the wafer was stripped via plasma etching and a 1700-Å film of platinum (Pt) was sputtered to serve as a backside electrode during nanoporous Si electrochemical etching later in the fabrication process. Following Pt deposition, the front side of the wafer was patterned with photoresist and Si_3N_4 was etched away selectively to yield bare Si regions in preparation for nanoporous Si etching. Next, patterned thin-film heaters were deposited onto the wafer via e-beam evaporation comprising of 100, 1000, and 3800 Å of chrome (Cr), Pt, and gold (Au), respectively. Following heater deposition, ProTEK, an electrical insulating polymer, was spun coated onto the wafer and patterned with photoresist. The wafer was then O_2 plasma etched to leave only small square morphologies of ProTEK over two discrete areas of the thin-film igniter. Patterned square solder contact pads consisting of 100, 1000, 500, and 1000 thick films of Cr, Pt, Au, and copper (Cu) were then deposited on to the wafer. Following solder pad deposition, exposed Si was electrochemically etched in a solution of hydrofluoric acid (HF) (3 parts): ethanol (EtOH) (1 part):H_2O_2 (0.5% v/v) to produce nanoporous Si pits approximately 10 μm deep, which serve as a thermal insulating barrier between the thin-film heater and Si substrate. Detailed analysis of the nanoporous Si etching procedure can be found in other works (*12, 13*). An optical microscope photograph of a fabricated and diced ignition substrate chip is shown in figure 7.

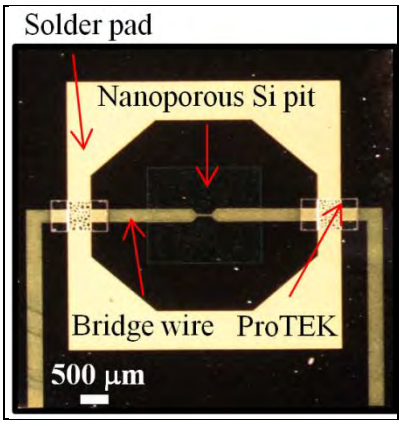

Figure 7. Photograph of fabricated and diced ignition substrate.

To verify the capacity of the heaters to reliably ignite a confined quantity of nanothermite, electrical characterizations of the electro-thermal heating elements used in these devices was conducted presented in other works (*14*).

The material chamber and fluid reservoirs are fabricated using p-type Si double polished wafers and starts with depositing a patterned solder pad with equivalent dimensions and positioning to the solder pad region located on the ignition substrate wafer. Cleave lines, ports for wire bonding, and material chamber/fluid reservoir cavities are then deep reactive ion etched (DRIE) in the wafer.

The nozzle caps were fabricated on a p-type [100] orientation Si wafer double side coated with 600-nm-thick films of Si_3N_4. Solder pads were initially deposited on the wafer to provide alignment marks for subsequent processing and a method to bond nozzles onto the fluid reservoirs. Si_3N_4 was etched from the top side of the wafer selectively to leave bare Si pits for potassium hydroxide (KOH) etching. The wafer was then submerged in a 45% solution of KOH heated to 90 °C for 8 h to etch approximately 250-μm-deep cavities with angular side walls. Following KOH etching, the wafer was inverted and subjected to backside DRIE to produce 150-μm-diameter ejection ports.

Following wafer processing, single dice from each wafer were cleaved to facilitate individual device assembly. Material chambers and fluid reservoirs were submerged in a heated solution of ethylene glycol containing a molten 47 °C melting point solder alloy. The molten solder preferentially wetted the metallic features on each dice resulting in a uniform solder coating on to the exposed solder pads. Following solder coating, the material chamber and fluid reservoir were brought into contact with the ignition substrate and nozzle dice, respectively, in a heated solution of ethylene glycol to bond the two chips together. Optical microscope photographs of the assembled ignition substrate/material chamber chip and fluid reservoir/nozzle chip are shown in figure 8.

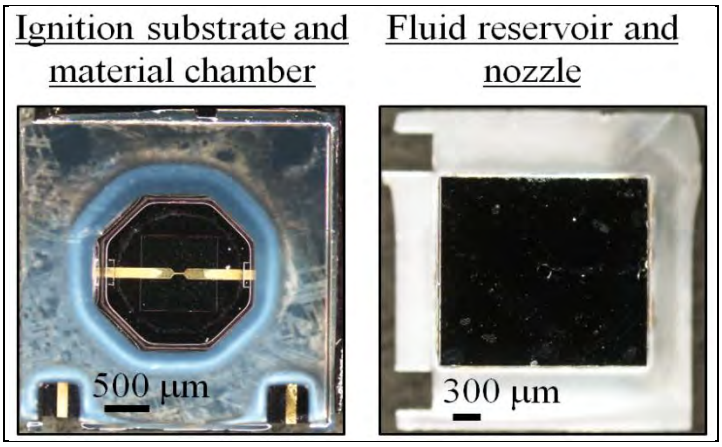

Figure 8. Two piece partial assembly of a nanoenergetic micro-fluidic jet injector: ignition substrate bonded with a material chamber (left) and fluid reservoir bonded with a nozzle (right).

PDMS membranes were prepared by mixing Sylgard 184 Si base (10 parts) with a curing agent (1 part) thoroughly in a glass beaker. The mixture was then degassed under vacuum for 1 h and spun coated at 1000 RPMs for 90 s on Kapton taped glass substrates. Kapton was used as opposed to glass to minimize chemical interactions between the PDMS and substrate as it cures, facilitating an easy film transfer. The PDMS was allowed to cure at room temperature for 24 h and individual sections were measured, and then cut and peeled from the Kapton substrate to use for assembling complete devices. The PDMS membranes were manually aligned and brought into contact with the material chamber/ignition substrate chip and then subsequently with the fluid reservoir/nozzle chip. Van der waals forces provided a PDMS reversible bond, which successfully assembled complete devices together. A photograph of two assembled nanoenergetic micro-fluidic jet injectors next to a U.S. dime is shown in figure 9.

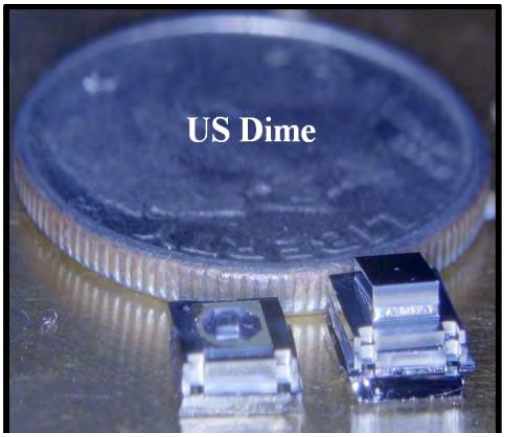

Figure 9. Assembled nanoenergetic micro-fluid jet injectors: without nozzle (left) and with nozzle (right).

Although the PDMS bonding procedure used to assemble these devices results in relatively weak interfacial bonds, more robust device bonding can be achieved in the future by using a combination of O_2 plasma treatments (to produce hydrophilic hydroxyl radicals on the surface of PDMS) and epoxy bonding.

4. Summary and Conclusions

We have demonstrated the fabrication of first generation nanoenergetic micro-fluidic jet injectors assembled from the cleaved dice of four separately processed Si wafers. The devices may be integrated with nanoenergetic material and previous experiments have verified the capacity of the electro-thermal heater to provide controlled and repeatable ignition. In the future, tightly bound devices will be filled with CuO/Al nanothermite and the mechanical deflection of the PDMS membrane will be evaluated against modeled behaviors to locate an ideal PDMS membrane thickness. Following these experiments, the fluid reservoir/nozzle chip will be filled with dyed water and subjected to various characterization methods to extract critical device operating parameters such as jet ejection velocity, jet diameter, fluid dispersion, and penetration depth.

5. References

1. Mitragotri, S. Current Status and Future Prospects of Needle-free Liquid Jet Injectors. *Nat Rev Drug Disc.* **2006**, 543–548.
2. Stachowiak, J. C. Piezoelectric Control of Needle-free Transdermal Drug Delivery. *Journal of Controlled Release* **2007**, *124*, 88–97.
3. Arora, A.; Prausnitz, M. R.; Mitragotri, S. Micro-scale Devices for Transdermal Drug Delivery. *International Journal of Pharmaceutics* **2008**, 364, 227–236.
4. Morris, Christopher; Currano, C. J.; Zakar, E. Nanoenergetic Materials for Energy Conversion Applications. *European MRS Symposium,* Strasbourg, France, 2009.
5. Currano, L. J.; Churaman, W. Energetic Nanoporous Silicon Devices. *JMEMS* **2009**, *18*, 799–807.
6. Shende, Rajesh et al. Nanoenergetic Composites of CuO Nanorods, Nanowires, and Al-Nanoparticles. *Propellants, Explosives, Pyrotechnics* **2008**, *33*, 122–130.
7. Fischer, S. H.; Grubelich, M. C. Theoretical Energy Release of Thermites, Intermetallics, and Combustible Materials. *Sandia National Labs* (Albuquerque, NM, USA), 1998.
8. Cooper, P. W.; Kurowski, S. R. *Introduction to the Technology of Explosives,* 1996.
9. Young, W. C.; Budynas, R. G. *Roark's Formulas for Stress and Strain,* 2001.
10. Schneider, F. et al. Mechanical Properties of Silicones for MEMS. *Journal of Micromechanics and Microengineering* **2008**, *18*, 065008.
11. Mata, A.; Fleischman, A. J.; Roy, S. Characterization of Polydimethylsiloxane (PDMS) Properties for Biomedical Micro/Nanosystems. *Biomedical Microdevices* **2005**, *7*, 281–293.
12. Becker, C. R.; Apperson, S. J.; Morris, C. J.; Gangopadhyay, S.; Currano, L. J.; Churaman, W.; Stoldt, C. R. Galvanic Porous Silicon Composites for High-velocity Nanoenergetics. *Nanoletters* **2010**, *11*, 803–807.
13. Becker, C. R.; Currano, L. J.; Churaman, W.; Stoldt, C. R. Thermal Analysis of the Exothermic Reaction Between Galvanic Porous Silicon and Sodium Perchlorate. *ACS Applied Materials and Interfaces* **2010**, *2*, 2998–3003.
14. Staley, C. S. et al. Silicon-based Bridge Wire Micro-chip Initiators for Bismuth Oxide-aluminum Nanothermite. *Journal of Micromechanics and Microengineering* article in press, 2011.

List of Symbols, Abbreviations, and Acronyms

Al	aluminum
Al_2O_3	aluminum oxide
Au	gold
Cr	chrome
Cu	copper
$CuCl_2$	copper chloride
CuO	copper oxide
CuOH	copper hydroxide
DI	deionized
DRIE	deep reactive ion etched
EtOH	ethanol
HF	hydrofluoric acid
KOH	potassium hydroxide
MEMS	micro-electromechanical system
NaCl	sodium chloride
NaOH	sodium hydroxide
PDMS	polydimethylsiloxane
PEG	polyethylene glycol
Pt	platinum
Si	silicon
Si_3N_4	silicon nitride
TMD	Theoretical Maximum Density

NO. OF COPIES	ORGANIZATION
1 ELEC	ADMNSTR DEFNS TECHL INFO CTR ATTN DTIC OCP 8725 JOHN J KINGMAN RD STE 0944 FT BELVOIR VA 22060-6218
1 CD	OFC OF THE SECY OF DEFNS ATTN ODDRE (R&AT) THE PENTAGON WASHINGTON DC 20301-3080
1	US ARMY RSRCH DEV AND ENGRG CMND ARMAMENT RSRCH DEV & ENGRG CTR ARMAMENT ENGRG & TECHNLGY CTR ATTN AMSRD AAR AEF T J MATTS BLDG 305 ABERDEEN PROVING GROUND MD 21005-5001
1	US ARMY INFO SYS ENGRG CMND ATTN AMSEL IE TD A RIVERA FT HUACHUCA AZ 85613-5300
1	COMMANDER US ARMY RDECOM ATTN AMSRD AMR W C MCCORKLE 5400 FOWLER RD REDSTONE ARSENAL AL 35898-5000
1	US GOVERNMENT PRINT OFF DEPOSITORY RECEIVING SECTION ATTN MAIL STOP IDAD J TATE 732 NORTH CAPITOL ST NW WASHINGTON DC 20402
1	CLAY STALEY 5107 CHARITON DR COLUMBIA MO 65202
9	US ARMY RSRCH LAB ATTN RDRL D OFFICE OF DIRECTOR ATTN IMNE ALC HRR MAIL & RECORDS MGMT ATTN RDRL CIO LL TECHL LIB ATTN RDRL CIO MT TECHL PUB ATTN RDRL SER L B PIEKARSKI ATTN RDRL SER L C MORRIS (2 HCS) ATTN RDRL SER L L CURRANO (2 HCS) ADELPHI MD 20783-1197